# Decay of spatially periodic patterns in a nematic liquid crystal

Nándor Éber,* Stanislaw A. Rozanski,† Szilárd Németh, and Ágnes Buka
*Research Institute for Solid State Physics and Optics, Hungarian Academy of Sciences, P.O. Box 49, H-1525 Budapest, Hungary*

Werner Pesch and Lorenz Kramer
*Institute of Physics, University of Bayreuth, D-95440 Bayreuth, Germany*
(Received 18 August 2004; published 23 December 2004)

A detailed theoretical and experimental analysis of the decay of electroconvection patterns is presented in a planarly aligned nematic liquid crystal. The relaxation time is measured as a function of the wave number of the pattern using a light diffraction technique. A theoretical analysis exhibits a rich structure of the dispersion curves for the decay rates. An interesting relation between the realistic case of no-slip boundary conditions and the simpler free-slip case is found. The experimentally determined relaxation rates for both "conductive" and "dielectric" initial patterns follow the theoretical solution with subsequent jumps between branches when the wave number is increased.

DOI: 10.1103/PhysRevE.70.061706 PACS number(s): 61.30.Gd, 61.30.Dk, 47.54.+r, 42.25.Fx

## I. INTRODUCTION

Systems far from equilibrium often respond to excitations by creating spatially periodic patterns. Anisotropic fluids—like nematic liquid crystals—are especially rich in pattern forming phenomena [1]. The mean orientation of the elongated nematic molecules or, equivalently, the local optical axis is described by the director $\mathbf{n}$ with $\mathbf{n}^2=1$. Electroconvection (EC) driven by an ac voltage applied across a thin (thickness $d\sim 10-100$ $\mu$m) nematic layer is a common example of pattern forming instabilities [2]. EC is a threshold phenomenon which usually occurs as a primary instability in a slightly conducting nematic with negative dielectric and positive conductivity anisotropies (or vice versa [3,4]). The pattern then appears at onset in the form of a periodic array of parallel convection rolls (wave number $q$) coupled to a periodic modulation of the director orientation, which results in a sequence of dark and bright stripes observable in a microscope. Varying the easily tunable control parameters like the ac voltage (rms amplitude $V$, frequency $f$), magnetic field, temperature, etc., a wide variety of scenarios can be generated which makes electroconvection a popular model system for pattern formation studies. In particular the characteristic wave number $q$ of the patterns depends sensitively on $f$.

When the excitation is turned off the roll pattern decays as the system returns to its equilibrium (usually homogeneous) state. Though the relaxation time $\tau$ characterizing this decay process gives important insight into the nematohydrodynamic mechanism, it has so far not been analyzed systematically. It will be demonstrated in this paper, where we focus in particular on the dependence of $\tau$ on $q$ that such an analysis gives interesting new insights.

The various mechanisms responsible for EC are active on different characteristic time scales. The slowest time scale is given by the director relaxation time $\tau_d=\gamma_1 d^2/K_{11}\pi^2$, which sets the time scale for director reorientations, where $\gamma_1$ denotes the rotational viscosity and $K_{11}$ is the splay elastic modulus. The charge relaxation time $\tau_q=\epsilon_0\epsilon_\perp/\sigma_\perp$ is considerably shorter than $\tau_d$ ($\epsilon_\perp$ is the dielectric permittivity and $\sigma_\perp$ the conductivity component perpendicular to the director). The viscous relaxation time $\tau_{visc}=d^2/\nu$ characterizing the viscous damping ($\nu$ is the kinematic viscosity) of flow is much shorter than the other time scales, so the velocity field can be treated adiabatically. In some situations (not considered here), when one is, for instance, in (or near to) the regime where traveling waves appear at onset, the treatment of a nematic as an Ohmic conductor is insufficient. Then an additional time scale related to the recombination of charge carriers $\tau_{rec}$ becomes relevant (weak electrolyte model [5]).

Ideally all of the above processes contribute to the decay time, making the process very complex. Fortunately the fast processes (charge relaxation and the viscous damping) contribute only at the very beginning of the decay process, whereas the only relevant time scale at the later stage of the relaxation process is expected to be $\tau_d$. Thus, the process is expected to be rather universal, independent of the excitation mechanism. In fact, the only relevant quantity determining the long-time decay should be the wave number $q$, which (ideally) remains unaltered during the decay. Comparing the theoretical predictions with experiments could even be used to determine material parameters such as the viscosity (Leslie) coefficients.

The theoretical task of determining the asymptotic decay times of a pattern with nonzero wave number is in principle straightforward and conceptionally less complicated than the problem of EC, since only the director deformation and the flow field (back flow) are involved. In addition the pattern amplitudes continuously decrease when the decay process advances; thus, the analysis can be based on the linearized nematohydrodynamic equations. Nevertheless, so far the problem has been treated in the literature only in a "single mode" approximation (SMA) where the boundary conditions for the velocities are not implemented properly [6,7].

*Electronic address: eber@szfki.hu
†On leave from Higher Vocational State School in Pila, ul. Podchorazych 10, PL-64920 Pila, Poland.

 

Experimental studies of EC patterns are most often based on recording and digital processing of (stationary) shadowgraph images in a polarizing microscope. In the present experiment we have to resolve fast decay of low contrast (small deformations) patterns. The standard 25 Hz (or slower) video rate of common analog and/or digital cameras imposes a strong constraint on the recording speed and the typical 8-bit video digitization may also not provide sufficient gray-scale resolution. The shadowgraph technique is therefore less appropriate for the analysis of the decay process unless special instrumentation is used.

On the other hand, EC patterns represent a periodic optical grating. Illuminating them with a monochromatic (laser) light beam results in a diffraction pattern. The intensity $I_n$ of the $n$th-order fringe is for not too large pattern amplitude $\vartheta_m$ (i.e., the maximum tilt angle of the director) given by

$$I_n = B_n[J_n(Q\vartheta_m)]^2, \tag{1}$$

where $J_n$ is a Bessel function of the first kind of order $n$, while the quantities $B_n$ and $Q$ depend on the refractive indices, the angle of incidence, and the shape of the director profile [11,12]. In the limit of small $\vartheta_m$, which is relevant for our study, we have $I_n \propto \vartheta_m^{2n}$. Thus the $I_n$ for small $n$ prevail. For symmetry reasons only the even-order fringes are visible (at least for small deformations) at normal light incidence [8–11]. For oblique incidence [11,12], however, the odd-order fringes (in particular $n=1$) become accessible, which thus present a sensitive tool to monitor variations of EC pattern amplitudes near the threshold.

Based on these considerations an interesting optical method has recently been proposed to measure the relaxation times $\tau$ by diffraction on EC patterns [7]. The initial roll pattern has been induced by periodically switching the dc voltage between positive, zero, and negative values. The intensities of low-order fringes have been recorded, which have shown a sawtoothlike modulation due to the periodic reorientation of the director (growth and decay of the pattern), and the relaxation time has been obtained by fitting to results of the SMA approach. The method has only been applied to a single switching frequency of the excitation where $\tau$ is claimed to match the theoretical value. The analysis would have been more convincing if by varying the switching frequency the wave number $q$ of the EC pattern (which is a crucial parameter for $\tau$) had been systematically changed.

The approach in Ref. [7] has some disadvantages. First, it captures only the beginning of the decay process where one cannot expect a single time exponent to govern the dynamics. Furthermore, the theoretical analysis makes use of the SMA, which, although quite effective for the description of the EC state near threshold, is questionable for the relaxation process.

The work presented in this paper has two aims. On the one hand, the experimental technique was improved, using sine-wave ac voltage excitation that allowed us to measure the wavelength dependence of the relaxation times in a wide $q$ range. Moreover, we focused on the late stage of the relaxation process, which was expected to be determined by the largest relaxation time. On the other hand, we present a rigorous theoretical analysis of the relaxation time problem with proper handling of the boundary conditions. The results given in Sec. II reveal some surprising features.

We want to stress again that although the pattern was created by electroconvection, the relaxation occurred in the absence of an electric field. Thus the results obtained are valid for the decay of any other patterns which are characterized by periodic splay-bend deformation of the director (e.g., shear-flow-induced convection rolls).

## II. THEORY OF THE DECAY

The system under study is a nematic layer of thickness $d$ confined by plates parallel to the $x$-$y$ plane. We assume strong planar anchoring of the director at the bounding plates in the $x$ direction, so in the rest (i.e., basic) state the director $[\mathbf{n}=(n_x,n_y,n_z)]$ is given as $\mathbf{n}=(1,0,0)$. We consider a situation where a spatially periodic pattern with wave vector $\mathbf{q}=(q,p)$ in the $x$-$y$ plane has been generated—e.g., by electroconvection. We will discuss in general terms the relaxation process after switching off the excitation. One is then left with the standard nematodynamic equations for the Cartesian components of the director field $\mathbf{n}$ and of the velocity field $\mathbf{v}=(v_x,v_y,v_z)$; see, e.g., [13–15]. We will use dimensionless units. The unit of length is chosen to be $d/\pi$, time is measured in units of the director relaxation time $\tau_d$, and elastic moduli are scaled with the splay elastic constant $K_{11}$ and viscosity coefficients by the rotational viscosity $\gamma_1$.

Here, we restrict ourselves to normal roll patterns with $p=0$ (no $y$ dependence). Thus all fields depend only on $x$ and $z$. The $y$ components of $\mathbf{n}$ and $\mathbf{v}$ vanish. In the nematodynamic equations linearized about the basic state, which are sufficient for the late stage of the decay process the dependence on $x$ becomes harmonic—e.g, $n_z(x,z,t)=\overline{n_z}(z,q,t)\sin(qx)$ and $v_z(x,z,t)=\overline{v_z}(z,q,t)\cos(qx)$. Since the decay process is slow compared to the viscous relaxation time $\tau_{visc}$, time derivatives of $\mathbf{v}$ can be (adiabatically) neglected. After eliminating $v_x$ with the help of the incompressibility condition $\boldsymbol{\nabla}\cdot\mathbf{v}=0$ we arrive at the following linear equations:

$$[\partial_t + K_{33}q^2 - \partial_z^2]q\overline{n_z}(z,q,t) - [\alpha_2 q^2 + \alpha_3\partial_z^2]\overline{v_z}(z,q,t) = 0, \tag{2}$$

$$[\alpha_2 q^2 + \alpha_3\partial_z^2]q\partial_t\overline{n_z}(z,q,t) - [\eta_2\partial_z^4 - \eta_r q^2\partial_z^2 + \eta_1 q^4]\overline{v_z}(z,q,t) = 0, \tag{3}$$

where

$$\eta_1 = (-\alpha_2 + \alpha_4 + \alpha_5)/2, \quad \eta_2 = (\alpha_3 + \alpha_4 + \alpha_6)/2,$$

$$\eta_r = \eta_1 + \eta_2 + \alpha_1 \tag{4}$$

are effective (Miesowicz) shear viscosities. Note that the correction to $n_x=1$ (basic state) vanishes at linear order.

These equations have to be supplemented with realistic rigid boundary conditions—i.e., strong planar anchoring of the director and no slip for the velocities at the bounding plates at $z=\pm\pi/2$ in dimensionless units:

$$\overline{n_z} = 0, \quad \overline{v_z} = 0, \quad \partial_z \overline{v_z} = 0 \quad \text{at} \quad z = \pm \pi/2. \tag{5}$$

The last condition follows from $v_x(\pm\pi/2)=0$ and $\boldsymbol{\nabla}\cdot\mathbf{v}=0$.

The velocity component $\overline{v_z}$ can be eliminated, yielding a partial differential equation for the director component $\overline{n_z}(z,q,t)$:

$$[(\alpha_2 q^2 + \alpha_3 \partial_z^2)^2 - (\eta_2 \partial_z^4 - \eta_r q^2 \partial_z^2 + \eta_1 q^4)] q \partial_t \overline{n_z}(z,q,t) - [\eta_2 \partial_z^4 - \eta_r q^2 \partial_z^2 + \eta_1 q^4](K_{33} q^2 - \partial_z^2) q \overline{n_z}(z,q,t) = 0. \tag{6}$$

Equation (6) allows modal solutions in exponential form $\overline{n_z}(z,q,t) = n(s,q) e^{-\mu t} e^{isz}$ [analogously one has $\overline{v_z}(z,q,t) = v(s,q) e^{-\mu t} e^{isz}$]. Thus we arrive from Eq. (6) at the following dispersion relation:

$$(\alpha_2 q^2 - \alpha_3 s^2)^2 \mu + (\eta_2 s^4 + \eta_r q^2 s^2 + \eta_1 q^4)(K_{33} q^2 + s^2 - \mu) = 0. \tag{7}$$

Clearly Eq. (7) involves only two independent variables $s^2/q^2$ and $\mu/q^2$. Obviously one can superpose modes with $s$ and $-s$ to yield real solutions with a given parity (reflection symmetry in $z$). From Eq. (2) we see that the amplitudes $n(s,q)$ and $v(s,q)$ of the modal solutions are related by

$$n(s,q) = G(s,q) v(s,q), \tag{8}$$

with

$$G(s,q) = \frac{\alpha_2 q^2 - \alpha_3 s^2}{q(K_{33} q^2 + s^2 - \mu)}. \tag{9}$$

In a rigorous treatment one has to take into account that Eq. (7) is a cubic equation in $s^2$, which provides three roots ($s_1^2$, $s_2^2$, and $s_3^2$) for each $\mu$ and $q$ which are to be superposed to satisfy the realistic no-slip boundary conditions. We expect that only situations where $\overline{n_z}$ and $\overline{v_z}$ are even functions of $z$ will be of relevance. Thus, the exact solution of the decay problem is a linear combination of cosine functions constructed from the roots of Eq. (7),

$$\overline{n_z}(z,t) = e^{-\mu t} N(z) = e^{-\mu t} \Sigma_{j=1}^3 A_j G_j \cos(s_j z),$$

$$\overline{v_z}(z,t) = e^{-\mu t} V(z) = e^{-\mu t} \Sigma_{j=1}^3 A_j \cos(s_j z), \tag{10}$$

with $G_i = G(s_i, q)$ calculated from Eqs. (8) and (9). Combining Eq. (5) with Eq. (10) a set of three homogeneous linear equations are obtained for the weights $A_1$, $A_2$, and $A_3$. A nontrivial solution exists if the corresponding determinant vanishes. Thus one obtains a discrete eigenvalue spectrum $\mu_k(q^2)$, $k=1,2,\ldots$ with the corresponding eigenfunctions $N_k(z)$ and $V_k(z)$ [see Eqs. (10)]. As to be expected the $\mu_k$ are found to be real and positive. We will order them in increasing magnitude ($\mu_1 < \mu_2 < \cdots$) in the following.

Before we discuss the resulting eigenvalue spectrum in detail, which requires numerical calculations, we will address the situation in the SMA. This case is obtained by replacing the last condition in Eq. (5) by $\partial_z^2 \overline{v_z} = 0$, which corresponds to the unrealistic case of zero tangential stress on the velocity field ("free slip"). Then the even eigenfunctions $N_k(z)$, $V_k(z)$ are proportional to $\cos(S_k z)$ with $S_k = 2k-1$, $k = 1,2,3,\ldots$, independent of $q^2$. Thus the $s$ in the dispersion relation can be identified with $S_k$ and for the free-slip eigenvalues $\overline{\mu_k}(q^2)$ one obtains

$$\overline{\mu_k} = \frac{\hat{\mu}_k}{1 - b_k}, \quad \text{with} \quad \hat{\mu}_k = S_k^2 + K_{33} q^2,$$

$$b_k = \frac{(\alpha_2 q^2 - \alpha_3)^2 S_k^2}{\eta_2 S_k^4 + \eta_r q^2 S_k^2 + \eta_1 q^4}. \tag{11}$$

Note that $\overline{\mu_1}$ coincides with the growth rate (properly nondimensionalized) on which the analysis in Ref. [7] was based [see Eq. 7 there]. Also note that $\hat{\mu}_k$ presents a set of purely elastic (no-back-flow) decay rates. Thus $\hat{\mu}_1$ gives the slowest decay mode in this limit of vanishing viscosities. The (positive) quantities $b_k$ describe the enhancement of the decay by back flow. Whereas $\hat{\mu}_1$ should underestimate the actual decay constant, $\overline{\mu_1}$ is expected to give a bound from above, since the free-slip boundary conditions are less restrictive than the rigid ones to the flow field.

A surprising feature appears when the higher branches $\overline{\mu_k}$ of the SMA are considered. Figure 1(a) displays the ten first branches ($\overline{\mu_1}, \ldots, \overline{\mu_{10}}$) as a function of $q^2$ for the parameter set of Phase 5/5A listed in Table I. One sees that the "natural" ordering $\overline{\mu_1} < \overline{\mu_2} < \overline{\mu_3} < \cdots$ applies only for small $q^2$. With increasing $q^2$ the higher-indexed branches $\overline{\mu_k}(q^2)$ cross all the lower-indexed ones. Thus, each branch becomes the lowest within some interval of $q^2$. The explanation for this behavior is that for the slowest mode the spatial variation along $x$, characterized by $q$, is balanced by a corresponding variation along $z$, characterized by $S_k$. Clearly there exists an envelope, which bounds all SMA branches from below. For large $q^2$ the envelope becomes a straight line through the origin whose slope is determined by the minimum of $\overline{\mu_k}/q^2$ for large $q^2$ minimized over $k$. This minimum is obtained by treating $S_k$ as a continuous variable and minimizing $\overline{\mu_k}$, which gives $min(\overline{\mu_k}/q^2) = \Xi = 4.2285$ at $S_k^2 = 1.0493 q^2$ for our material parameters.

Returning to the rigorous eigenvalue spectrum $\mu_k(q^2)$, Fig. 1(b) displays the lowest ten branches ($\mu_1, \ldots, \mu_{10}$) as a function of $q^2$ (solid and dash-dotted lines, parameter set of Phase 5/5A). The decay rates $\overline{\mu_1}$ (SMA) and $\hat{\mu}_1$ (no back flow) are also shown (dashed and dotted lines, respectively). The rigorous solution offers modes with smaller eigenvalues $\mu_k$ (longer decay) than $\overline{\mu_1}$. In fact the lowest branch $\mu_1(q^2)$ remains below $\overline{\mu_1}(q^2)$ for any $q^2$; see also the inset [actually, $\mu_1(q^2)$ remains below all $\overline{\mu_k}(q^2)$; see below]. As expected, $\hat{\mu}_1$ gives a lower bound. For $k>1$, each $\mu_k$ branch crosses $\overline{\mu_1}$ at some $q^2$ and in that neighborhood the slope increases and approaches that of $\overline{\mu_1}$, so that the two curves remain close to each other (with $\overline{\mu_1} > \mu_k$) in some $q^2$ interval. For $k = 2,3,\ldots$ these intervals follow each other and build up an almost continuous line running just below $\overline{\mu_1}$ (for large $k$ the effect becomes more pronounced).

More generally, the branches $\mu_k(q^2)$ consist of alternate pieces with higher and lower slopes forming a steplike curve. The branches do not touch or cross each other. One notices a close similarity with the structure of the SMA curves in Fig. 1(a). There, however, the curves cross each other. Substantial

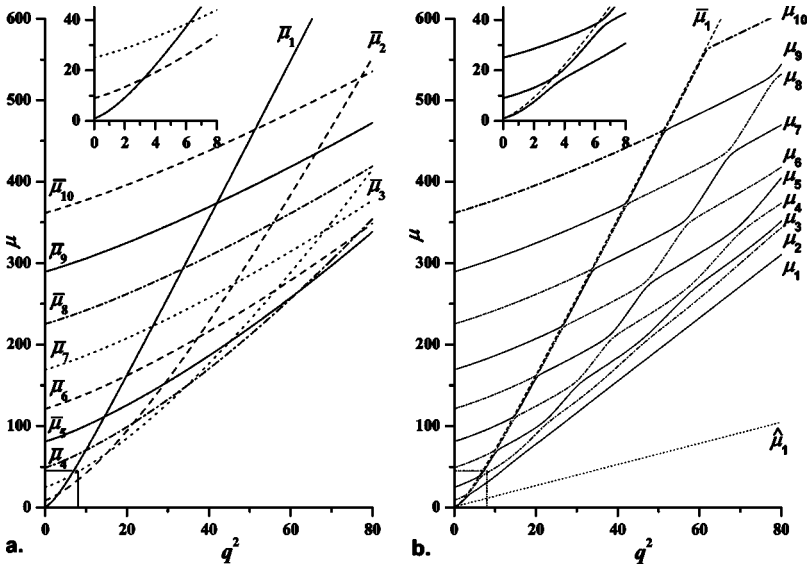


FIG. 1. Theoretical values of the dimensionless decay rate of the director distortion versus dimensionless $q^2$ calculated for the parameter set of Phase 5/5A. (a) The ten lowest $\overline{\mu_k}$ branches of the dispersion relation for the case of free-slip boundaries [see Eq. (11)]. (b) The ten lowest $\mu_k$ branches of the dispersion relation obtained from the rigorous calculation are depicted by solid (for odd $k$) and by dash-dotted (for even $k$) lines. Also shown are dashed and dotted lines corresponding to the SMA branch $\overline{\mu_1}$ and to the flow-free case ($\hat{\mu}_1$), respectively. The insets show the corresponding lowest three branches for low $q^2$ with an enlarged scale.

deviations occur only in the vicinity of the crossing points of the branches $\overline{\mu_k}(q^2)$. In fact, it is quite common in physics that a dispersion relation is composed of crossing branches in some "unperturbed" approximation while the rigorous solution of the same problem results in combination of the branches and gap formation at the crossing points (see, e.g., the electronic band structure in crystals in the nearly free electron limit). Here the unperturbed problem corresponds to the free-slip case. Indeed, for $q^2 \gg 1$, the influence of no-slip boundary conditions is in effect a small perturbation that becomes important near the points of degeneracy (the crossings) of the unperturbed eigenvalues.

It follows from Eq. (10) that the eigenmodes $N_k(z,q)$, $V_k(z,q)$ are not simple harmonic functions of $z$. In Fig. 2 the function $N_1(z)$ is shown for the lowest branch $\mu_1$ at $q^2=1$, 10, and 100. At small $q$, where $\mu_1$ is close to $\overline{\mu_1}$, one has $N_1(z) \sim \cos(z)$. This changes drastically as $q$ increases, where $N_1(z)$ eventually develops into a boundary layer (this is the case for $k=1$ only; see below). In general we can identify an index $k_0$ associated with a certain $q^2$ interval where $\mu_{k_0}$ is close to $\overline{\mu_1}$. Within that interval the corresponding eigenmodes $N_{k_0}(z)$ are dominated by a contribution $\sim\cos(z)$ superimposed with oscillations $\sim\cos(2k_0 z)$ of small amplitude. To the left of those intervals the contribution $\sim\cos(z)$ eventually vanishes and the eigenmodes are dominated by a fast oscillation $\sim\cos[(2k_0-1)z]$. To the right of those intervals the $\cos(z)$ contribution shifts towards $\cos(3z)$ though with small amplitude superimposed with a strong $\sim\cos[(2k_0+1)z]$. The profiles $N_{10}(z)$ shown in Fig. 3 for $q^2=58$ (inside the interval $k_0=10$), 40 (below interval), and 76 (above interval) demonstrate this effect. More generally, the eigenfunctions on the $j$th steep portion of the $\mu_k$ branches become approximately proportional to $\cos[(2j-1)z]$ with $j=1,2,\ldots$, while on the next flat portion a $\cos\{[2(k+j)-1]z\}$ dependence dominates. One may conclude that an exact eigenfunction $N_j(z,q)$ is similar to a SMA eigenfunction $\cos(2k-1)z$ whenever the eigenvalue $\mu_j(q^2)$ is near to $\overline{\mu_k}(q^2)$.

Interestingly, for not too small $q^2$, the lowest branch $\mu_1$ remains separated from the rest (and separated from all SMA branches). This can be understood most easily by looking, in the limit $q^2 \to \infty$, at the quantity $\min(\overline{\mu_k}/q^2)=\Xi$ from another side. $\Xi$ corresponds to the point where $\mu/q^2$, as given in the dispersion relation, Eq. (7), as a function of $s^2$, has a minimum—i.e., where two roots $s_1^2$ and $s_2^2$ of the dispersion relation coincide (note that the $s_i^2$ scale with $q^2$). Below this point ($\mu/q^2 < \Xi$) the dispersion relation has two complex conjugate roots $s_1^2$ and $s_2^2$ and a negative root $s_3^2$. Thus all $s_1$, $s_2$, and $s_3$ have (substantial) imaginary parts so that the $e^{is_j}$ decay rapidly either to the left or to the right depending on

TABLE I. The material parameters of the nematic Phase 5/5A used for the numerical calculations.

| Quantity | Unit | Value at 30 °C | Reference |
|---|---|---|---|
| $K_{11}$ | $10^{-12}$ N | 9.8 | [16] |
| $K_{33}$ | $10^{-12}$ N | 12.7 | [16] |
| $\alpha_1$ | $10^{-3}$ N s/m$^2$ | −39 | [16] |
| $\alpha_2$ | $10^{-3}$ N s/m$^2$ | −109.3 | [17,16] |
| $\alpha_3$ | $10^{-3}$ N s/m$^2$ | 1.5 | [16,17] |
| $\alpha_4$ | $10^{-3}$ N s/m$^2$ | 56.3 | [16,17] |
| $\alpha_6$ | $10^{-3}$ N s/m$^2$ | −24.9 | [16,17] |

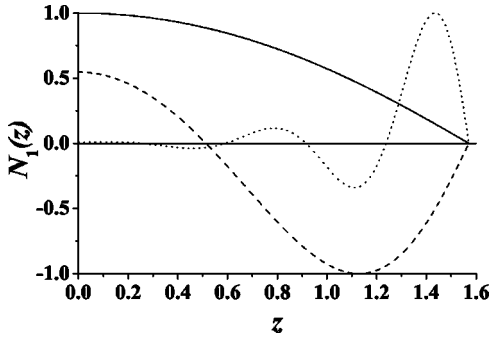


FIG. 2. Normalized director profile $N_1(z)$ corresponding to the $\mu_1$ mode calculated for the parameter set of Phase 5/5A at $q^2=1$ (solid line), 10 (dashed line), and 100 (dotted line), respectively.

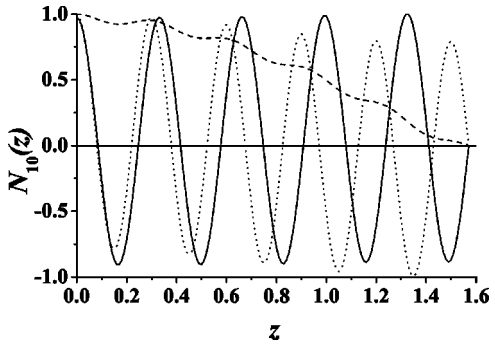


FIG. 3. Normalized director profile $N_{10}(z)$ corresponding to the $\mu_{10}$ mode calculated for the parameter set of Phase 5/5A at $q^2=40$ (solid line), 58 (dashed line), and 76 (dotted line), respectively.

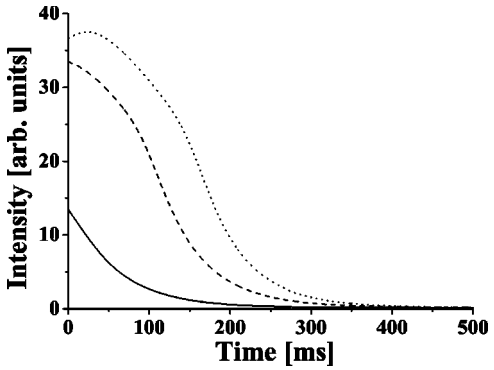


FIG. 4. Temporal evolution of the light intensity of the first-order diffraction fringe $I_1$ following the shutdown of the applied voltage in a 28-$\mu$m-thick cell of Phase 5A at $f=1200$ Hz. Curves with different line styles correspond to different initial pattern amplitudes set by the dimensionless control parameter $\varepsilon=0.009$ (solid line), 0.019 (dashed line), and 0.066 (dotted line), respectively.

the choice of sign. Then one can construct, at some value of $\mu$ $(=\mu_1=3.8801q^2)$, a solution of the problem that decays away from either boundary and which represents a boundary layer solution. For $\mu/q^2>\Xi$ the complex conjugate pair becomes real. Near $\Xi$ their difference is small and their superposition describes a slowly modulated, rapidly oscillating function (the rapidly decaying contribution from $s_3$ remains localized near to the boundary). This gives the branches $\mu_2,\mu_3,\ldots$, which are characterized by an increasing number of modulation periods. In the limit of large $q^2$ they form a quasicontinuum, well separated from $\mu_1$.

Knowledge of the decay rates is not sufficient to describe the decay process fully. First, one needs the initial state before switching off the voltage, which involves solving the full linear (for small $\epsilon$) EC problem as a function of frequency for the given nematic. This is numerically cumbersome, in particular in the "dielectric" (large-$q$) regime. The initial condition determines the expansion coefficients $A_i$ [see Eq. (10)]. Since the eigenvalue problem Eqs. (2) and (3) is not self-adjoint, one has to solve the adjoint problem as well. Finally the contribution of the different modes to the intensity of the fringes has to be calculated following—e.g., the methods presented in [10,11]. A corresponding detailed analysis is presently under way.

### III. EXPERIMENT

In order to cover a large range of decay rates $\mu$ and/or wave numbers $q^2$, the decay of EC patterns was investigated in planar samples of the commercial nematic mixtures Phase 5 and Phase 5A(Merck). The latter is a doped version possessing higher electrical conductivity. These substances are popular in the investigation of EC, since they are chemically stable and their material parameters are well characterized [17,16].

Planar cells were assembled using rubbed polyimide coated electrode surfaces made by E.H.C. Co. The transparent indium tin oxide (ITO) electrodes covered a surface of 1 cm$\times$1 cm. The thickness $d$ of the cells was adjusted by nylon spacers and was determined by a standard interferometric method before filling.

EC was driven by sinusoidal voltage synthesized by a function generator PC card through an electronic switch and a high-voltage amplifier. This switch allowed an abrupt (within 10 $\mu$s) shutting down of the applied voltage. The actual ac voltage across the sample was measured by a digital voltmeter.

The sample was thermostatted by a PC-controlled Instec hot-stage at $T=30.0\pm0.05$ °C. A beam of a laser diode of wavelength $\lambda=650$ nm illuminated the cell on an area of about 1 mm$\times$2 mm. In the state of electroconvection a highly regular diffraction pattern could be observed as a sequence of light spots on a screen placed normal to the beam at a distance of $L=660$ mm. As the hot stage could be rotated around an axis in the plane of the cell perpendicular to the director, diffraction at normal as well as at oblique incidence of light could be investigated. Depending on the applied voltage diffraction fringes up to the ninth order could be seen. At higher voltages, however, the diffraction spots gradually became diffuse, indicating the reduction of pattern regularity (appearance of defects above the threshold for secondary instabilities), and finally faded into an almost uniformly scattering background (the turbulent, dynamic scattering mode).

The higher sensitivity of diffraction at oblique incidence could be clearly demonstrated by the fact that a couple of diffraction orders were still visible at low voltages where no fringes could be seen at normal incidence. Therefore the measurements shown were carried out at an angle of incidence $\beta=5$ °.

In EC one usually observes two types of patterns, "conductive" and "dielectric" rolls. In the first regime (at frequencies $f$ below the cutoff frequency $f_c$) the director distortion is virtually stationary and the dimensionless $q$ is of the order of 1, while in the latter regime $(f>f_c)$, $n_z$ follows the external ac frequency and $q\gg1$ can easily be obtained. $f_c$ is roughly proportional to the electric conductivity of the sample.

Using Phase 5A in a cell of $d=28$ $\mu$m thickness EC patterns of the conductive type existed in a wide frequency range (10–1380 Hz). For $f>1200$ Hz the threshold of the EC patterns grew steeply with the frequency. Thus the highest accessible frequency (which was still below the cutoff) was practically limited by the maximum sinusoidal output

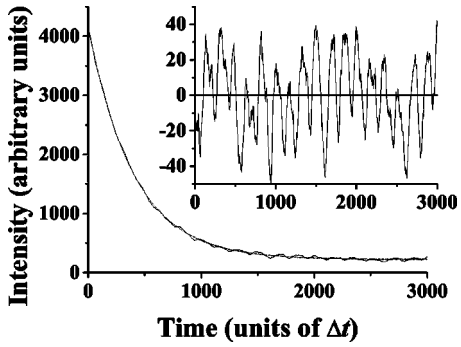


FIG. 5. The tail of a typical decay curve (solid line) with a fitted exponential (dash-dotted line). The inset shows the residuals to the single-exponential fit at an enlarged scale.

voltage ($\pm 160 V_{\text{peak}}$) the high-voltage amplifier could provide which was too low to enter into the dielectric regime. Normal rolls—i.e., fringes along a single line parallel to the director—appeared above the Lifshitz point $f_L$. At low frequencies ($f < f_L \approx 200$ Hz) oblique rolls were observed which resulted in diffraction fringes aligned along two crossing lines as expected.

The wavelength of the pattern varied from $\Lambda = 47.4$ $\mu$m at low $f$ to $\Lambda = 16.6$ $\mu$m at the highest $f = 1380$ Hz. The dimensionless $q^2$ fell into the range 1.4–11.3. At lower $f$ the accuracy of $q^2$ was mainly determined by the precision of distance measurements on the screen, while at higher frequencies the increase of the fringe diameter was the main limiting factor.

In order to study the large-$q$ regime we investigated the decay of the dielectric rolls in a thinner ($d = 9.2$ $\mu$m) cell filled with Phase 5 having much lower electric conductivity. The dielectric regime occurred above $f_c \simeq 100$ Hz. The low-frequency conductive regime with oblique rolls occuring up to $f_L \simeq 60$ Hz has not been examined in detail. The wavelength of the dielectric rolls was substantially smaller than in the conductive regime (as expected) and could be tuned from $\Lambda = 4.6$ to 2.9 $\mu$m by increasing the frequency. In dimensionless units a range from $q^2 = 14$ to 38 has been covered. At these smaller $\Lambda$ the diffraction angles were higher and thus fewer number of fringe orders were visible. In general the diameters of the diffraction spots corresponding to the dielectric rolls were noticeably larger, indicating less regular patterns. Note that the conductivities of the two samples and the thickness of the cells have been chosen in such a way that the (dimensionless) wave numbers $q$ in the two regimes joined almost continuously (see also Fig. 7).

In order to study the decay of electroconvection patterns the intensity of the diffracted light was monitored. An optical fiber (with a diameter of 1 mm) which was positioned at the center of the selected fringe (typically the first-order one) transmitted the diffracted light into a photomultiplier working in its linear regime. Its output was fed through a current-to-voltage converter into a 16-bit analog-to-digital (AD) converter card. That allowed recording of the intensity at high precision with adjustable sampling rate.

As already mentioned in the Introduction, the light intensity $I_n$ of an $n$th-order fringe is proportional to $\vartheta_m(t)^{2n}$. Hence, assuming an exponential decay of the deformation ($\vartheta_m = \vartheta_0 e^{-t/\tau}$) the characteristic time for the intensity decay of the $n$th-order fringe is given by $\tau_n^* = \tau/2n$. Thus higher-order fringe intensities decay faster; moreover, their intensities ($\propto \vartheta_0^{2n}$) are smaller and more sensitive to nonlinear corrections. Consequently, we carried out a detailed analysis of $I_1$ which is accessible in the case of oblique incidence.

The wavelength $\Lambda$ of the EC pattern can conveniently be tuned by the frequency $f$ of the excitation. At each $f$ first the EC threshold voltage $V_c$ was determined based on visibility criteria. Then the voltage $V$ was raised by 1% which corresponds to a value of $\varepsilon = (V^2 - V_c^2)/V_c^2 = 0.02$ of the dimensionless control parameter. At this $\varepsilon$ typically four diffraction orders were visible. $\Lambda$ was then determined by measuring the distances $D_n$ between the $n$th-order diffraction fringes and the main beam (zeroth order) and using the condition for constructive interference,

$$\Lambda[\sin\beta + \sin(\alpha_n - \beta)] = n\lambda, \tag{12}$$

where $\beta$ is the angle of incidence and $\alpha_n = \arctan(D_n/L)$ is the diffraction angle for the $n$th-order fringe.

The detector was then positioned at the center of the first-order fringe (to the place of maximum intensity) to monitor temporal variations. Data acquisition was started at the instant of switching off the applied voltage. Figure 4 shows some examples of the decay curves obtained when starting from different $\varepsilon$ values. Note that the fringe intensity is not expected to grow monotonically with $\varepsilon$ (although $\vartheta_m$ does so), as the Bessel function in Eq. (1) is an oscillating function of its argument. The dotted curve in Fig. 4 indicates that at $\varepsilon = 0.066$ the deformation is already large enough to get past the first maximum of Eq. (1) which explains the slight increase of the intensity at the initial part of the decay.

In order to focus on small deformations, however, during measurements the gain of the AD converter was increased by a factor of 8. Furthermore, we zoomed in on the tail (on values below 1/16 of full scale) of the relaxation curve. This tail section which showed an exponential decay was finally recorded as 3000 points with a 12-bit resolution. The sampling time was chosen so that the recorded section corresponded to a period of about $(6-7)\tau_1^*$. Before processing the data they were smoothed by a sliding averaging involving 51 neighboring data points. This improved the signal-to-noise ratio considerably while it did not affect the exponential shape of the curve. Finally the relaxation time of the fringe intensity, $\tau_1^* = \tau/2$, was obtained by a least-squares fitting of a single exponential. Figure 5 depicts an example of the recorded data and the fitted exponential. The mean square deviation of the experimental data from the fitted curve is typically less than 1% of the full scale, and hence a systematic deviation is almost undetectable in the figure.

Despite the good fit, the relaxation times $\tau$ obtained from repeated recordings showed a typical scattering of about 10% which may be attributed to variations of the initial EC state. Actually one expects that the existence of wave number gradients of the order of 10% is consistent with the width of the stable wave number band at $\varepsilon \approx 0.02$ of our initial state. By averaging over the decay times of ten consequtive measurements at the same frequency we obtained an average

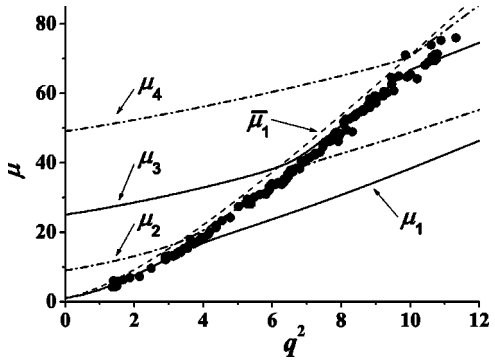


FIG. 6. The dimensionless decay rate $\mu$ of the director versus dimensionless $q^2$. The four lowest $\mu_k(q^2)$ branches of the dispersion relation are depicted alternatingly by solid (for odd $k$) and by dash-dotted (for even $k$) lines. The dashed line shows the expectation of the SMA $[\overline{\mu_1}(q^2)]$. Solid circles are the data $\mu_{expt}$ measured at sinusoidal excitation for Phase 5A in the conductive regime.

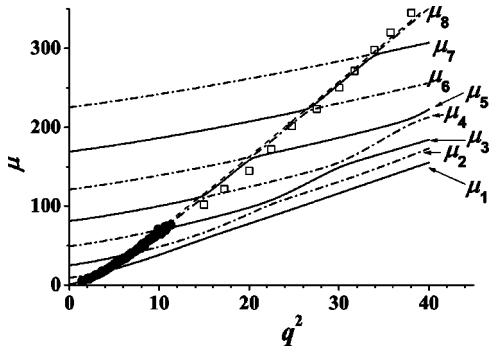


FIG. 7. The dimensionless decay rate $\mu$ of the director versus dimensionless $q^2$. The eight lowest $\mu_k(q^2)$ branches of the dispersion relation are depicted alternatingly by solid (for odd $k$) and by dash-dotted (for even $k$) lines. The dashed line shows the expectation of the SMA $[\overline{\mu_1}(q^2)]$. Solid circles and open squares are the data $\mu_{expt}$ measured at sinusoidal excitation in the conductive regime of Phase 5A and in the dielectric regime of Phase 5, respectively.

$\overline{\tau}$. Finally the dimensionless decay rate was calculated by scaling it with the director relaxation time ($\mu_{expt}=\tau_d/\overline{\tau}$).

The procedure above could not be fully applied to the thin cell in the dielectric regime. As a consequence of the smaller wavelength of the dielectric rolls (which is independent of $d$ and is a combination of material parameters), their relaxation time turned out to be quite short (0.14–0.48 ms) compared to the minimum sampling time (0.01 ms) of the high-resolution AD converter card. Therefore in this case a digital oscilloscope with an 8-bit resolution was used to record the temporal evolution of the fringe intensity and all recorded points (except those saturating due to overdriving at the start of the decay) were included in the exponential fitting.

## IV. COMPARISON OF EXPERIMENTAL DATA WITH THEORY

Figure 6 displays the measured data together with the theoretical curves in the conductive range. Focusing on the very end of the relaxation process we expected that there the system decays with the slowest rate $\mu_1$ in the whole $q$ range because faster modes die out earlier. It can be seen, however, that the measured points do not follow the lowest branch of the dispersion relation (the slowest decaying mode) except in the very-low-$q^2$ range up to about 4. Neither do they follow the predictions of the SMA as all points are below that curve. There are, however, distinct ranges of $q^2$ where $\mu_{expt}$ data lie almost perfectly on one of the branches provided by the rigorous calculation (on $\mu_1$ for $q^2<3.5$, on $\mu_2$ for $5.0<q^2<6.7$, and on $\mu_3$ for $8.0<q^2<10.0$).

Figure 7 displays the measured decay rates together with the theoretical curves for the whole $q$ range, including the dielectric mode. The trend of the persistent switching of $\mu_{expt}$ to higher-$\mu_k$ branches with increasing $q^2$ continues in the dielectric regime. This similarity is actually not surprising. Although the electroconvecting state in the dielectric regime is crucially different from that of the conductive one (e.g., the director tilt follows the excitation frequency which can be nicely detected in the oscillating intensity of the diffraction fringes), the decay itself occurs under the same field-off condition in both cases.

These data indicate that the assumption of the final decay occurring with the slowest mode does not hold or at least cannot be justified with the spatiotemporal resolution facilitated by our experimental setup. Surprisingly the slowest mode $\mu_1$ is not reflected in the diffracted light intensity (except for small $q^2$). Instead the decay rate $\mu_k(q^2)$ with the eigenfunction $N_k(z)$ closest to $\cos(z)$ (with small superimposed oscillations as shown in Fig. 3) dominates. Apparently this eigenfunction has the largest overlap with the initial director field and thus provides the largest weights $A_i$. With increasing $q^2$ this eigenfunction appears at higher indices $k$ of the eigenvalues $\mu_k$. As a result the system switches from one branch to the next. For $q^2$ in the switching region the measured $\mu_{expt}$ falls in between the branches indicating the absence of a single dominating mode. Actually fitting the decay curves with a superposition of more exponentials reduces the mean-square deviation slightly in those regions. Preliminary calculations which follow the general scheme presented at the end of Sec. II, show indeed that for $q^2=10$ (conductive regime; see Fig. 6) where $\mu\approx\mu_3$ the contribution of this mode to the fringe intensity $I_1$ is larger by a factor 30–50 compared to the contribution of the modes $\mu_1$ and $\mu_2$.

## V. CONCLUSIONS

A rigorous theoretical solution has been provided for the problem of the decay modes of periodic patterns in nematic liquid crystals. The proper handling of the boundary conditions has yielded a dispersion relation with a sequence of modes with different relaxation times in contrast to the single-exponential decay predicted by the slowest SMA mode. The branches of the dispersion relation have been calculated for the nematic liquid crystal Phase 5/5A.

Laser diffraction at an oblique incidence has turned out to be an excellent tool to monitor the decay process experimen-

tally. The decay rates have been measured in a wide wave number range. Several distinct $q$ ranges have been found where the relaxation of the pattern is characterized by an exponential decay slightly slower than that given by the SMA, but coinciding with one of the calculated branches of the dispersion relation. That indicates that the generally multimode decay is usually dominated by a single mode though somewhat different from that provided by the SMA. This trend holds for both the conductive and dielectric regimes, showing that the type of excitation has only a minor influence on the decay process. The detailed analysis of the impact of the initial conditions including a theoretical decomposition into modes is still under investigation.

## ACKNOWLEDGMENTS

Financial support by Hungarian Research Grant Nos. OTKA-T031808, OTKA-T037336, and OM00224/2001 and the EU Research Training Network PHYNECS is gratefully acknowledged.

[1] *Pattern Formation in Liquid Crystals*, edited by Á. Buka and L. Kramer (Springer-Verlag, New York, 1996).

[2] L. Kramer and W. Pesch, in *Pattern Formation in Liquid Crystals*, edited by Á. Buka and L. Kramer (Springer-Verlag, New York, 1996), pp. 221–255.

[3] A. Buka, B. Dressel, W. Otowski, K. Camara, T. Toth-Katona, L. Kramer, J. Lindau, G. Pelzl, and W. Pesch, Phys. Rev. E **66**, 051713 (2002).

[4] A. Buka, B. Dressel, L. Kramer, and W. Pesch, Phys. Rev. Lett. **93**, 044502 (2004).

[5] M. Treiber and L. Kramer, Mol. Cryst. Liq. Cryst. Sci. Technol., Sect. A **261**, 311 (1995).

[6] R. A. Rigopoulos and H. M. Zenginoglou, Mol. Cryst. Liq. Cryst. **35**, 307 (1976).

[7] P. L. Papadopoulos, H. M. Zenginoglou, and J. A. Kosmopoulos, J. Appl. Phys. **86**, 3042 (1999).

[8] H. M. Zenginoglou and J. A. Kosmopoulos, Appl. Opt. **28**, 3516 (1989).

[9] J. A. Kosmopoulos and H. M. Zenginoglou, Appl. Opt. **26**, 1714 (1987).

[10] H. M. Zenginoglou and J. A. Kosmopoulos, J. Opt. Soc. Am. A **14**, 669 (1997).

[11] T. John, U. Behn, and R. Stannarius, Eur. Phys. J. B **35**, 267 (2003).

[12] H. M. Zenginoglou and J. A. Kosmopoulos, Appl. Opt. **27**, 3898 (1988).

[13] P. G. de Gennes, *The Physics of Liquid Crystals* (Clarendon Press, Oxford, 1974).

[14] S. Chandrasekhar, *Liquid Crystals* (Cambridge University Press, Cambridge, England, 1992).

[15] H. Pleiner and H. R. Brand, in *Pattern Formation in Liquid Crystals*, edited by Á Buka and L. Kramer (Springer-Verlag, New York, 1996), pp. 15–67.

[16] M. Treiber, N. Éber, Á. Buka, and L. Kramer, J. Phys. II **7**, 649 (1997).

[17] H. H. Graf, H. Kneppe, and F. Schneider, Mol. Phys. **77**, 521 (1992).